

GPU-accelerated Linear Algebra for Coupled Solvers in Industrial CFD Applications with OpenFOAM

Stefano Oliani^{1*}, Ettore Fadiga¹, Ivan Spisso¹, Luigi Capone¹,
Federico Piscaglia²

¹Leonardo S.p.a, Via Pieragostini 80, Genova, Italy.

²Dept. of Aerospace Science and Technology, Politecnico di Milano, Italy.

*Corresponding author(s). E-mail(s): stefano.oliani.ext@leonardo.com;
stefanooliani95@gmail.com;

Abstract

The present work describes the development of heterogeneous GPGPU implicit CFD coupled solvers, encompassing both density- and pressure-based approaches. In this setup, the assembled linear matrix is offloaded onto multiple GPUs using specialized external libraries to solve the linear problem efficiently. These coupled solvers are applied to two industrial test cases representing common scenarios: the NASA CRM in a transonic regime [1] and the external aerodynamics study of the DriveAER car [2]. Significant performance enhancements are evident when compared to their CPU counterparts. Specifically, the NASA CRM case achieves an overall speedup of more than 4x, while the DriveAER test case demonstrates improved stability and reduced computational time compared to segregated solvers. All calculations were carried out utilizing the GPU-based partition of the `davinci-1` supercomputer at the Leonardo Labs, featuring 82 GPU-accelerated nodes.

Keywords: GPU Acceleration, implicit density-based coupled solver, implicit pressure-based coupled solver, OpenFOAM, AmgX

1 Introduction

The justification for utilizing GPUs in CFD simulations lies in their highly efficient massively parallel technology and impressive performance per watt [3–5]. Given the distinctive architectural variances between GPUs and CPUs, the development of specialized algorithms becomes imperative to fully harness the potential performance of GPU hardware [6–11]. Given the relatively recent emergence of this field, there remains significant scope for enhancing the acceleration of these solutions.

There are primarily two approaches to accelerate CFD simulations. The first approach entails a comprehensive overhaul of the CFD code, specifically optimized for exclusive execution on Graphics Processing Units (GPUs). Although this method often yields significant speed improvements, it comes with trade-offs. It typically demands a considerably longer development period and is highly tailored to address a specific problem, referred to as a “full port”. The alternative approach involves adopting a partial-offloading strategy, where only the computationally intensive portions of the code are transferred to the GPU. There are already many examples in which fast GPU simulations have been demonstrated for unstructured finite-volume CFD software using the full or partial offloading strategy [9–12].

In CFD software packages, steady-state simulations for external aerodynamics are typically carried out using either pressure-based or density-based solvers. The choice between these solvers depends on the flow speed. While implicit density-based solvers present a coupled structure by nature, pressure-based solvers can be divided into SIMPLE-based and coupled methods. The SIMPLE operation follows a segregated approach, addressing linear systems for individual physical variables like pressure and velocity components, one at a time. While this approach has limited memory requirements, it often results in slow convergence, requiring a substantial number of iterations [13]. When implementing a partial port strategy for SIMPLE-based solvers, a significant portion of the overall solution time is spent transferring data between the host (CPU) and the GPU for each linear solver. Consequently, the overall performance gains from this strategy tend to be limited to around a 2x speedup [9]. To overcome these limitations, the exploration of coupled solvers [14–16] emerges as a promising avenue for implementing the partial port strategy on GPUs. Compared to segregated solvers, coupled solvers offer notable advantages, including linear scalability of CPU time with cell count and the capacity to achieve more rapid convergence of residuals, particularly for steady-state flows. Implicit coupled solvers typically combine robustness, stability and a reduced number of nonlinear iterations required for the convergence, especially for steady-state problems. These features result in a significantly improved overall convergence of the solver. This statement is counter-balanced by the increased size of a linear system of algebraic equations that needs to be solved in the coupled solution, as well as the increase in computer storage and computational effort per block solution. Current advancements in computer technology have led to the availability of powerful machines and a strong push towards achieving exascale performance in numerical simulation codes. These developments have significantly altered the trade-off between memory requirements and simulation speed, particularly when dealing with computational meshes that consist of hundreds of millions of computational points.

Historically, the practical application of coupled solvers on GPUs in large-scale industrial settings faced a significant hurdle due to the traditional constraints on GPU hardware’s memory capacity. The motivation for the current development work lies in the focus on the attention to modern GPU cards, which are characterized by enhanced memory capacity and adeptness in handling the computational demands of industrial workflows [17]. This ongoing effort is therefore centered on the adaptation of existing CFD workflows to fully exploit the capabilities offered by contemporary GPU technology. Open-source tools are proving to be valuable assets for industrial CFD applications. In this context, OpenFOAM [18] is the most widely employed open-source tool for CFD simulations in Academia and Industry [19]. In the author’s knowledge, despite several effort have been made of either density- and pressure-based implicit coupled solvers in OpenFOAM [14, 20–22], implicit coupled solvers are not available in the official distributions of the software [23, 24]. While significant efforts have been made to accelerate linear algebra in SIMPLE-based solvers [9] and to accelerate combustion calculations [25], there are currently no investigations of performance obtained through partial offload strategy on GPUs of coupled solvers in the OpenFOAM framework.

We present a study on the performance of implicit coupled linear algebra GPU offloading for the *ICSFoam* library [20]. The study encompasses results obtained from both an implicit compressible density-based solver and an incompressible pressure-based coupled solver. These solvers are applied to two industrial test cases that represent typical scenarios. Specifically, the implicit compressible density-based coupled solver is applied to the NASA CRM in a transonic regime [1], while the pressure-based implicit coupled solver is employed for the external aerodynamics of the DriveAER car [2]. The goal of this work is to assess the acceleration of a GPGPU CFD solver based on the OpenFOAM framework. In this approach, the algebraic solution of the assembled coupled matrix from the discretization of the flow transport problem is offloaded onto multiple GPUs. This strategy is expected to significantly enhance the computational performance of external aerodynamics simulations across various flow speeds.

The paper is structured as follows: in Sec. 2, we provide a brief overview of the methodology used to assemble coupled matrices for the pressure and density-based algorithms employed in this study. Additionally, we outline the strategy adopted for GPU offloading of linear algebra using the NVIDIA *AmgX* library [8]. Sec. 3 provides a summary of the hardware and techniques utilized for the performance assessment. In Sec. 4, we present the results for two test cases with industrial relevance. The simulations are initially validated by comparing them to experimental data and other computational fluid dynamics (CFD) solutions. Subsequently, the performance benefits from the presented implementation are discussed. Finally, conclusions from the study are drawn in Sec. 5.

2 Methodology

An in-house version of the *ICSFoam* library [20] was used for this work. The library was developed starting from the *HiSA* solver [26] as a generalization of OpenFOAM

for arbitrary systems of implicitly coupled partial differential equations. A detailed description can be found in [20]. The library was initially designed for compressible turbomachinery flows [27], but was also employed for multiphysics aeroelastic simulations of transonic flutter [28]. In this section, a broad overview of the coupled pressure-based and density-based solvers used in this work is given before describing the linear algebra acceleration through *AmgX*.

In general, a linearized and discretized coupled system of equations is written as:

$$A_{ii}\mathbf{U}_i + \sum_N A_{ij}\mathbf{U}_j = \mathbf{b}_i \quad (1)$$

for a generic cell i of the mesh and its neighbours N . The coefficients, or blocks, can be seen as small sub-matrices of dimension $n \times n$, where n is the number of equations. In turn, each block is split into subblocks based on the coupling coefficients in terms of scalar and vector variables. This allows a very intuitive treatment of coupled systems and can be easily generalized to any number of variables. As an example, Fig. 1 shows this splitting for the incompressible Navier-Stokes equations, where one scalar and one vector equations are present.

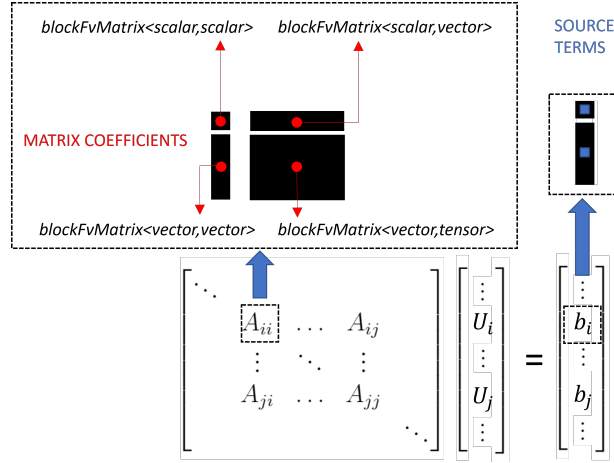


Fig. 1: Sub-blocks and source term structure for a system of coupled equations with one scalar and one vector variables.

For the solution of linear systems of equations in the CPU version of the code, the GMRES Krylov subspace solver [29] combined with the Lower Upper Symmetric Gauss-Seidel [30] preconditioner are used. This combination has proven a suitable approach in terms of efficiency and stability in density-based solvers for compressible Navier-Stokes equations.

2.1 Density-based solver

The three-dimensional compressible Reynolds-averaged Navier-Stokes (RANS) equations in conservation form can be written as:

$$\int_V \frac{\partial \mathbf{Q}}{\partial t} dV + \int_{\partial V} (\mathbf{F}_c - \mathbf{F}_v) dS = 0 \quad (2)$$

where

$$\mathbf{Q} = \begin{bmatrix} \rho \\ \rho \mathbf{u} \\ \rho E \end{bmatrix}, \mathbf{F}_c = \begin{bmatrix} \rho \mathbf{u} \cdot \mathbf{n} \\ (\rho \mathbf{u} \otimes \mathbf{u}) \cdot \mathbf{n} + p \mathbf{n} \\ \rho \mathbf{u} H \cdot \mathbf{n} \end{bmatrix}, \mathbf{F}_v = \begin{bmatrix} 0 \\ \boldsymbol{\tau} \cdot \mathbf{n} \\ (\boldsymbol{\tau} \cdot \mathbf{u} + \mathbf{q}) \cdot \mathbf{n} \end{bmatrix} \quad (3)$$

and \mathbf{n} is the face normal vector, ρ is the density, \mathbf{u} is the velocity, E is the total internal energy, H is the total enthalpy, p is the static pressure, $\boldsymbol{\tau}$ is the viscous stress tensor and \mathbf{q} is the heat flux vector. In the case of steady-state equations, the time derivative is replaced with a pseudo-time term τ in the equations. Using the finite volume method for the spatial discretization of Eqs. (2), we get a set of semi-discretized equations:

$$V \frac{\partial \mathbf{Q}}{\partial \tau} = \mathbf{R}(\mathbf{Q}) \quad (4)$$

When an implicit method is employed to march the equations in pseudo-time to the iteration $n + 1$, the residual is linearized about iteration n as

$$\mathbf{R}(\mathbf{Q}^{n+1}) \approx \mathbf{R}(\mathbf{Q}^n) + \left. \frac{\partial \mathbf{R}(\mathbf{Q})}{\partial \mathbf{Q}} \right|_{\mathbf{Q}=\mathbf{Q}^n} \Delta \mathbf{Q}^n, \quad \Delta \mathbf{Q}^n = \mathbf{Q}^{n+1} - \mathbf{Q}^n \quad (5)$$

At each iteration the following linear system is solved to compute the solution increment $\Delta \mathbf{Q}^n$:

$$\left[\frac{V}{\Delta \tau} \mathbf{I} - \left. \frac{\partial \mathbf{R}(\mathbf{Q}^n)}{\partial \mathbf{Q}^n} \right] \Delta \mathbf{Q}^n = \mathbf{R}(\mathbf{Q}^n) \quad (6)$$

Standard Newton iterations involving exact linearizations of the numerical flux $\mathbf{R}(\mathbf{Q})$ would give the best convergence rate for the nonlinear equations (4), but are very expensive to compute, if not impossible to evaluate. Therefore, approximate Jacobians are usually adopted in the linearization of the implicit part. In this work we adopt the approximate Jacobian formulation of Luo *et al.* [31], so that the contribution of each internal face to block coefficients can be expressed as:

$$A_{ii} = A_{ii} + \frac{\partial \mathbf{R}_{ij}(\mathbf{n}_{ij})}{\partial \mathbf{Q}_i} = A_{ii} + \frac{1}{2} S_f (\mathbf{J}(\mathbf{Q}_i, \mathbf{n}_{ij}) + |\lambda_{ij}| \mathbf{I}) \quad (7)$$

$$A_{ij} = A_{ij} + \frac{\partial \mathbf{R}_{ij}(\mathbf{n}_{ij})}{\partial \mathbf{Q}_j} = A_{ij} + \frac{1}{2} S_f (\mathbf{J}(\mathbf{Q}_j, \mathbf{n}_{ij}) - |\lambda_{ij}| \mathbf{I}) \quad (8)$$

where S_f is the face area, \mathbf{J} is the convective flux Jacobian and λ_{ij} is the sum of the spectral radii of the Roe and viscous flux matrices (see [32] for more details). The dependence on the surface outward-normal vector \mathbf{n}_{ij} pointing from cell i to cell j has been highlighted since caution must be taken according to the sign of the flux. Indeed one has that: $\mathbf{R}_{ij}(\mathbf{n}_{ij}) = -\mathbf{R}_{ji}(\mathbf{n}_{ji})$.

The MUSCL reconstruction-evolution approach is used to calculate the numerical flux residual term $\mathbf{R}(\mathbf{Q}_i)$. The first step involves primitive variables interpolation from cell centroids to face centers. TVD slope-limiters are used in the vicinity of shocks to avoid the appearance of spurious oscillations that may lead to stability issues. After the reconstruction, left and right states are used to compute the numerical flux through approximate Riemann solvers at each cell interface. Roe, HLLC and AUSM+Up approximate Riemann solvers are available in the ICSFoam library. Finally, integrating the fluxes over all faces of the cell (cfr. second term of Eq.2) we obtain the numerical flux residual $\mathbf{R}(\mathbf{Q}_i)$.

2.2 Pressure-velocity coupling for pressure-based solver

Originally, pressure-based algorithms were developed for incompressible flows in their segregated SIMPLE formulation [33] and then extended to the compressible regime [34]. They were originally developed in the 1970s and 1980s, when parallelism was limited, and computational resources were scarce. Consequently, numerical algorithms based on a segregated solution procedure gained popularity. In segregated algorithms, the pressure-velocity system are assembled by decoupling the momentum and pressure equations by treating the other unknown explicitly, using the value from the previous iteration; the equation set is solved sequentially, component by component and equation coupling is achieved through Picard iterations. Optimal segregated algorithms hold only a single matrix in memory and re-use its storage space. Such treatment of the pressure-velocity system is unnatural since the connection between the two variables is linear and can be resolved simultaneously in a single linear system. To achieve this goal, we want first to assemble a single linear system across the complete set of governing equations to simultaneously: a) couple p and u fields without simplification; b) remove the need for “inner” Picard iterations for p-u coupling and c) remove the need for under-relaxation.

Extensive literature is available on the derivation of coupled pressure-based solvers equations and the relative implementations. Incompressible and compressible formulations can be found for OpenFOAM as well [14, 15], even if no coupled solvers are currently available in the official release. Here, for the sake of simplicity, we will limit ourselves to the incompressible steady-state Navier-Stokes equations. Compressible pressure-based solvers are usually obtained by solving a segregated energy equation.

According to Eq.(1), the blocks of the system can be written explicitly as:

$$A_{ii} = \begin{bmatrix} \mathbf{a}_{ii}^{uu} & \mathbf{a}_{ii}^{up} \\ \mathbf{a}_{ii}^{pu} & a_{ii}^{pp} \end{bmatrix} \quad A_{ij} = \begin{bmatrix} \mathbf{a}_{ij}^{uu} & \mathbf{a}_{ij}^{up} \\ \mathbf{a}_{ij}^{pu} & a_{ij}^{pp} \end{bmatrix} \quad (9)$$

Where the sub-blocks splitting previously described is evident and: \mathbf{a}^{uu} is a 3x3 tensor representing the diagonal term of the momentum equation, \mathbf{a}^{up} and \mathbf{a}^{pu} are vectors representing the off-diagonal coupling terms, and a^{pp} is a scalar representing

the diagonal term of the pressure equation. In this section we derive formulas for these terms in the case of pressure-velocity coupling.

Following the derivation of Mangani *et al.*[14], the steady discretized momentum and continuity equations can be written as

$$\sum_N \mathbf{S}_f \left((\mathbf{u}_f \cdot \mathbf{n}) \mathbf{u}_f + p_f - \nu_{eff} \nabla \mathbf{u}_f \right) = 0 \quad (10)$$

$$\sum_N \mathbf{S}_f \cdot \mathbf{u}_f = 0 \quad (11)$$

Where the subscript f indicates values at cell faces and ν_{eff} represents the sum of laminar and turbulent viscosity. The convective term is linearized using $\mathbf{u}_f \cdot \mathbf{n}$ evaluated using previous iteration values. Here, due to the assumption of constant density, the pressure p is assumed to be normalized by the density ρ and therefore has dimension m^2/s^2 . The pressure equation is obtained using the discretized form of the continuity equation combined with the Rhie-Chow interpolation [35]:

$$\sum_N \mathbf{S}_f \cdot \left[\overline{\mathbf{u}_f} - \overline{\mathbf{D}_f} \cdot (\nabla p_f - \overline{\nabla p_f}) \right] = 0 \quad (12)$$

Where the overbar denotes linear interpolation from cell centroids to face centers and the operator $\mathbf{D} = V(\mathbf{a}_{ii}^{uu})^{-1}$, with V being the volume of the cell. This is needed to avoid checkerboard oscillations on collocated grids and results from the discretized momentum equation reconstructed at cell faces. We use $\|\mathbf{u}_f\|$ to indicate a generic first or second-order upwind discretization of the convective flux in the momentum equation. The surface-normal velocity gradient in the diffusive part of the momentum equation and the implicit pressure gradient in the pressure equation are evaluated using classical central-differencing with an explicit non-orthogonal correction for unstructured grids. For a detailed derivation of these terms, see [22]. With the above notation, the contribution of each internal face to the block coefficients is:

$$\begin{aligned} \mathbf{a}_{ij}^{uu} &= \left(-\|\mathbf{u}_f\| - \nu_{eff} \frac{\mathbf{S}_f \cdot \mathbf{n}}{\mathbf{n} \cdot \mathbf{d}_{ij}} \right) \mathbf{I} & \mathbf{a}_{ii}^{uu} &= \left(\|\mathbf{u}_f\| + \nu_{eff} \frac{\mathbf{S}_f \cdot \mathbf{n}}{\mathbf{n} \cdot \mathbf{d}_{ij}} \right) \mathbf{I} \\ \mathbf{a}_{ij}^{up} &= \mathbf{a}_{ij}^{pu} = (1 - f_x) \mathbf{S}_f & \mathbf{a}_{ii}^{up} &= \mathbf{a}_{ii}^{pu} = f_x \mathbf{S}_f \\ a_{ij}^{pp} &= \frac{(\overline{\mathbf{D}_f} \mathbf{S}_f) \cdot \mathbf{n}}{\mathbf{n} \cdot \mathbf{d}_{ij}} & a_{ii}^{pp} &= -a_{ij}^{pp} \end{aligned}$$

where f_x represents the linear interpolation weights and \mathbf{d}_{ij} is the distance vector between centroids of cells i and j .

2.3 AmgxCoupled4Foam

Even if performances of native GPU solvers can't be achieved, offloading only the linear algebra offers several advantages. First of all, a much smaller effort is needed in term of implementation to create the necessary coupling layer between the CFD solver

and the external linear algebra library. Second, the higher degree of flexibility and the possibility to test a wide variety of linear solvers. External linear algebra libraries offer a comprehensive set of linear solvers with competitive implementations, which are not usually available in proprietary CFD solvers. Third, the solution of the linear system is typically one of the most time-consuming part of the iteration, therefore accelerating this portion of the code alone allows to obtain relevant speedups.

As of now, one of the few concrete example of cutting-edge technology in the field of linear algebra solvers for GPUs is provided by NVIDIA through their open-source library, *AmgX* [8]. The *AmgX* library was chosen because it provides a comprehensive set of tools for solving large sparse system of equations arising from the discretization of differential equations on unstructured meshes. It features aggregation based algebraic multigrid methods for block coupled systems, along with several smoothers and preconditioners such as Gauss-Seidel, and incomplete-LU factorization. These can be combined with a variety of preconditioned Krylov subspace solvers are available, including GMRES and bi-conjugate gradient. Parallelism is achieved thanks to graph matching techniques and graph coloring algorithms. Moreover, the support already exists for the coupling with OpenFOAM segregated solvers [36], and has recently been tested for external aerodynamics and reactive flow simulations [9, 25]. Therefore, the coupling layer only needed to be adapted for coupled systems of equations and the underlying matrix structure of the ICSFoam library. Moreover, the library has already been tested successfully on the commercial solver ANSYS Fluent, leading to significant performance improvement for the solution of p-U coupling in pressure-based solvers. Indeed, finite-volume discretizations usually involve a compact stencil where only direct face-neighbours of the cell are involved, generating a very sparse matrix structure. Despite this fact, the matrix blocks are usually dense. This makes possible to leverage coalesced memory access on the GPU and obtain a more favorable arithmetic intensity compared to segregated solvers, achieving higher speedups of the linear system solution. In addition, since the system sparsity is not modified by the coupled or segregated nature of the solution, LDU addressing as well as row pointers and column indices for the CSR format are unchanged - the only difference being that now they refer to block entries instead of scalar coefficients. For scientific and computational applications, the CSR format can help to save memory and improve computational efficiency in operations involving large sparse matrices. CSR allows to access the matrix elements by saving only the indices of the first element of each row. This reduction in the number of indices translates directly to a reduction of the amount of data that have to be transferred from the main memory to the processors during Sparse Matrix Vector Multiplication (SpMVM) operations. The CSR matrix format is compatible with NVIDIA AmgX.

The library presented in this paper, named *amgxCoupled4Foam*, is linked dynamically at runtime when the simulation is started and allows to handle arbitrary coupled systems of equations through NVIDIA AmgX library on GPU accelerators. The v2112 ESI release of OpenFOAM is used in combination with CUDA Toolkit 11.4. The code structure follows best practice OpenFOAM coding guidelines, using a virtual constructor to select at runtime the desired linear solver. This allows, for example, to switch seamlessly between CPU legacy and AmgX GPU linear solvers without stopping the simulation.

The first aspect that must be taken into account is the flexibility given by the heterogeneous CPU/GPU paradigm. Consolidation of matrix partitions can be used to run simulations with an arbitrary number of GPUs and MPI ranks, provided the second is larger than the first. This is important because the part of the code that runs on the host can still benefit from increasing the number of CPU cores, without the necessity to increase the number of GPU devices as well. Indeed, several matrix partitions generated by different MPI ranks are consolidated on a root rank that sends compute requests to a single GPU device. This can be easily achieved by offsetting properly the row and column indices of each matrix partition to place the coefficients in the right position inside the consolidated matrix. This allows to fully benefit from increasing the number of CPU cores and GPU devices independently, balancing them to the user’s discretion. This type of flexibility of the heterogeneous approach finds no counterpart in the native GPU implementations. In the latter scenario, there is typically one MPI rank for each GPU device, so that the code must be completely revamped to port every single kernel on the accelerator. If this is not the case, even small code routines that are not accelerated can become significant bottlenecks in the code.

Algorithm 1 describes the steps needed to correctly transfer matrix coefficients to Amgx. Attention needs to be taken to fully exploit the block-coupled matrix structure in order to obtain better performances in the solution of the linear system. AmgX needs CSR block AoS format to carry out the solution of the linear system. This procedure is described schematically in Fig. 2. In the upper part of the figure, a small portion of the whole matrix is sketched, highlighting the division into sub-blocks. Incompressible Navier-Stokes equations are used as an example (4×4 blocks). Looping over each block of the matrix, the coefficients are linearized into an array in row-major format. Blocks are then concatenated to each other to obtain the array of coefficients in block AoS format. This array is then allocated and copied on the device, and a permutation CUDA kernel based on row and column indices is applied to convert the array to CSR format. A similar procedure, is also applied to convert the solution and the source term of the system in block AoS format, obtaining scalar array pointers. Permutation is not needed in this case since the pattern is implied.

An important remark concerns the exchange of boundary values on coupled patches, especially processor interfaces. Fig. 3 schematically shows the procedure for a simple domain with nine cells partitioned into three MPI ranks. In the lower part of the figure, the matrix sparsity pattern is shown for the serial matrix. For distributed matrices, arbitrary partitioning (obtained e.g. with SCOTCH or METIS) are dealt with by renumbering the mesh after decomposition. Halo layers are transferred from neighbour processors and included into the present matrix partition in CSR format using the local row number and global column index (in red in the figure). These coefficients are stored into arrays of size $N_{ExternalNZ}$ equal to the number of processor faces shared with neighbour partitions. For serial runs, this array is obviously empty, in absence of other kinds of coupled patches (e.g. cyclics). Please notice that, due to renumbering, the matrix sparsity pattern can change. This approach, however, makes the management of the distributed matrix much easier since each processor owns complete consecutive rows, so that there is no need to build and pass a partition

Algorithm 1 Procedure for coupled system solution offloading on AmgX

- 1: Convert source term and solution array from PtrLists of scalar and vector fields to block AoS format.
 - 2: **if** First iteration **then**
 - 3: Initialize AmgX with linear solver options and pass MPI communicators data to AmgX
 - 4: Map available devices on MPI ranks used by the application for consolidation
 - 5: **end if**
 - 6: Convert coupled matrix coefficients into block AOs format (Fig. 2)
 - 7: Exchange values with neighbour processor patches through MPI communications.
 - 8: **if** (First iteration or mesh topology has changed) **then**
 - 9: Setup rank-local and global number of rows so that AmgX can deal with matrix partitions
 - 10: Setup AmgX operations by uploading distributed row offsets, column indices and matrix values.
 - 11: **else**
 - 12: Replace the old matrix coefficients with new ones
 - 13: **end if**
 - 14: Permute matrix coefficients to obtain block CSR from LDU format.
 - 15: Upload solution and source term arrays on the device taking into account row offsets due to consolidation
 - 16: Call AmgX solver to solve the linear system
 - 17: Download solution array in block AoS format on the host. Each rank must read its portion of the consolidated solution.
 - 18: Get linear solver number of iterations and residuals on root rank and output them
 - 19: Retrieve solution array as PtrLists of scalar and vector fields from block AoS format
 - 20: **if** Final iteration **then**
 - 21: Free memory on the device and destroy AmgX objects
 - 22: **end if**
-

vector to AmgX. Instead, a trivial partitioning is implied where rows are consecutive in each rank and this is true independently of how the mesh is decomposed. The same approach is used for periodic conformal interfaces (*cyclic*s in OpenFOAM). In such case, eventual rotations between the coupled patches must be taken into account by multiplying the matrix coefficient by the corresponding transformation matrix.

3 Hardware and Applications

This section contains a general description of the testing procedure that has been applied to the libraries developed in the scope of this paper. In particular, the computing hardware is presented, together with a set of application cases that have been selected to evaluate the performance, the accuracy and the stability of the solvers.

The hardware selected for the computations is a set of GPU-accelerated nodes of the davinci-1 supercomputer [37]. This HPC system, recently installed at one

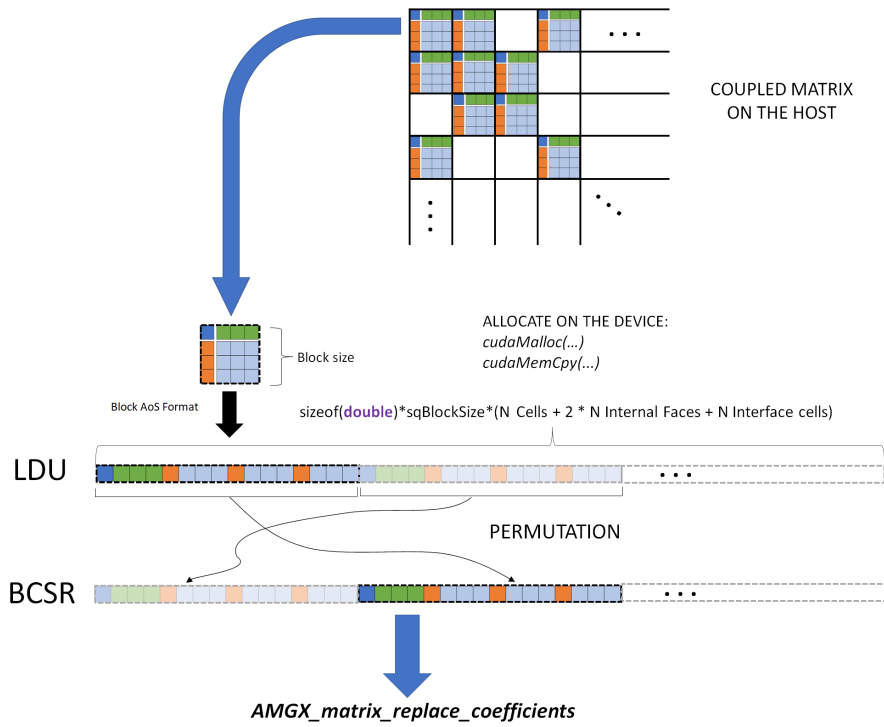


Fig. 2: Schematic procedure of coupled matrix values conversion into an array in block AoS format. Permutation of the blocks is needed to switch from OpenFOAM native LDU storage to block CSR format needed in AmgX.

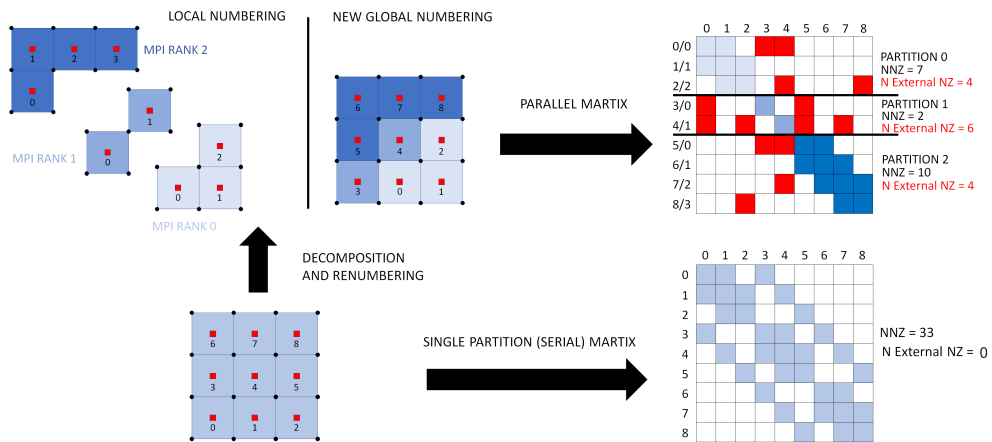


Fig. 3: Procedure for matrix partitioning and coupled processor patches coefficients insertion in distributed parallel matrix

of the Leonardo facilities in Genova, is equipped with 82 GPU-accelerated nodes characterized by:

- 2x24 cores AMD EPYC Rome 7402 Processor
- 512 GB total DRAM memory
- 4 x A100-SXM4-40GB NVIDIA GPUs
- 9.746 TFLOPS in FP64 (double) performance
- PCIe 4.0 x8 bus connection
- InfiniBand switches for nodes interconnection

More precisely, the authors have employed up to 18 nodes to test the performance and the scalability of both the pressure-based and the density-based solver. The availability of a considerable amount of computational resources has allowed the selection of application cases characterized by a level of complexity typical of industrial applications.

In section 4, the results of two open test cases will be presented to assess the correct implementation and the performance of the coupled solvers with GPU-accelerated linear algebra (GPU-LA from now on). The two cases are used to benchmark the density and pressure-based solvers, and present globally-accepted, widely adopted industrial geometries in the aerospace and automotive fields, respectively. These have been chosen from two widely known CFD workshops, so that comparison with available experimental data as well as results obtained with other state-of-art CFD software is possible.

Performance measurements are performed in a consistent manner for the two selected cases. First, simulations are run until convergence, monitoring residual values as well as aerodynamic coefficients. Then, the statistics are recorded for the following 500 iterations. Profiling is done by simply annotating the code outside the main computational kernels. For the present work, only the coupled system is offloaded on the device, while segregated turbulence equations are kept on the CPU. Future tests will investigate performance gaining attainable by offloading also turbulence equations.

It must be emphasized that the CPU version of the ICSFoam library is mainly a research code and is non-optimized for performances on many-core architectures. Therefore, it does not feature the most competitive implementation of iterative linear solvers. However, previous tests [20] showed that the CPU version of the code, though in general slower than other CFD codes, leads to acceptable computational times that are of the same order of magnitude of commercial codes. Put another way, the information on the speedup obtained with the GPU-LA version can be considered as fairly general and provides valuable insights into the attainable overall acceleration due to linear algebra offloading.

4 Results

4.1 Test Case 1: NASA CRM in transonic regime

The first test case presented regards the simulation of the NASA Common Research Model (CRM) [38] in the transonic flight configuration, from the AIAA Drag Prediction Workshop (DPW) 6. The CRM represents a modern commercial transport

airplane and was designed as a full configuration with a low wing, body, horizontal tail, and engine nacelles mounted below the wing. A summary of results obtained by the participants can be found in Tinoco *et al.*[39]. The full-scale geometry CAD is available on the workshop website [40], together with a number of overset, structured and unstructured meshes generated by the participants and by the committee. The wing-body-nacelle-pylon configuration was selected for the present study, also considering experimentally measured static aeroelastic deflections for an angle of attack of 2.75 degrees. This has been shown to dramatically improve predicted wing pressure distribution at transonic flight conditions [39]. Half-span of the full-scale model is simulated, by setting a symmetry condition on the corresponding plane. The domain is hexahedral with farfield surfaces placed 100 reference chords away from the aircraft. The simulated conditions are reported in Table 1, and aim at finding the predicted drag on the aircraft at a fixed lift coefficient $C_L = 0.5$. Two meshes generated by participants to the workshop were employed in this work: a coarse mesh of 45 million elements for scalability tests and comparisons between different linear solvers, and a fine mesh of about 260 million elements for comparison with experimental data and other solvers. Both meshes are unstructured and composed of mixed elements (hexahedra and tetrahedra with prismatic layers). Freestream conditions are imposed at far field boundaries, while a no-slip adiabatic condition is set at the walls. Simulations are run fully turbulent in “free air” configuration, without wind tunnel walls or support system. The baseline one-equation Spalart-Allmaras turbulence model [41] without rotation correction is employed.

Table 1: Simulated conditions for transonic CRM test case.

Quantity	Value
Mach Number	0.85
T_{ref}	300 K
p_{ref}	101 325 Pa
Re	$5e6$
C_L	0.5
Static Aeroelastic Deformation	2.75°
$\tilde{\nu}/\nu_\infty$	3

First of all, preliminary tests are conducted on the coarse mesh to verify that no discrepancies are present between the CPU and GPU version of the solver. As the linear solver, GMRES+LUSGS is used on the CPU, while GMRES with AMG preconditioner and Diagonal Incomplete Lower Upper (DILU) smoother is used for GPU-LA. Steady-state simulations are run for 10,000 iterations. Convergence of integral quantities was monitored for the CPU and GPU-LA runs. In Fig. 4, trends of drag and lift coefficients over the first 2500 iterations are shown. As can be noticed, the plots are almost superimposed, with very small differences shown in the upper and lower closeups on the right for the lift and drag coefficient, respectively. In both cases, a converged solution was already obtained after approximately 2000 iterations. This confirms that

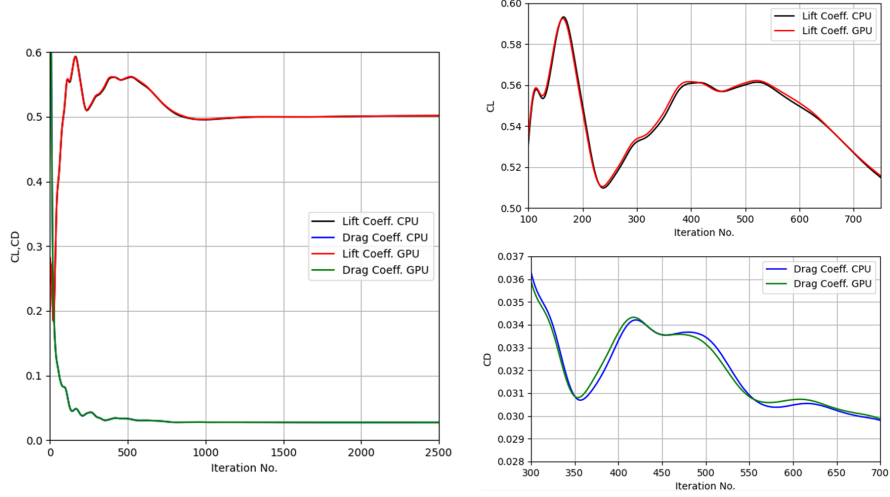


Fig. 4: Aerodynamic coefficients convergence history for the first 2500 iterations. CPU and GPU-offloaded linear algebra are represented. On the top and bottom right, close-up of lift and drag coefficient are shown, respectively.

iteration after iteration, the solution is identical no matter which linear solver is used for linear algebra.

Then, the accuracy of the results is assessed considering both integral quantities and pressure distributions across the aircraft surfaces.

Three versions of the drag coefficient are represented in figure 5, where total drag, pressure drag, and skin friction drag are compared to the results of other workshop participants. Outliers for which the predicted drag was too far from the average value (solid lines) are excluded from the figure, so that the resultant standard deviation (dashed lines) is quite small. The *ICSFoam* findings, marked by squares, are compared to all the other small dots representing the simulations executed with other CFD software. In particular, the final values lie within the standard deviation of the results from other participants and are considered satisfactory by the authors. An angle of attack of 2.57 degrees was used to obtain the target lift coefficient, which is also in agreement with other workshop participants. Pressure coefficients are extracted at six different wing spanwise location and compared with available experimental data from NASA Ames wind tunnel facility [1]. We can notice that the agreement is generally good throughout the wing, though some discrepancies are observed near the shock location at $\eta = 0.603$. This difference is completely confirmed by the results from other participants [39], where a significant spread in the shock intensity and location has been observed, which increases at higher angles of attack. These discrepancies are likely to be due to a significant amount of shock buffeting, observed in the experimental tests [39], that cannot be captured by steady state solutions.

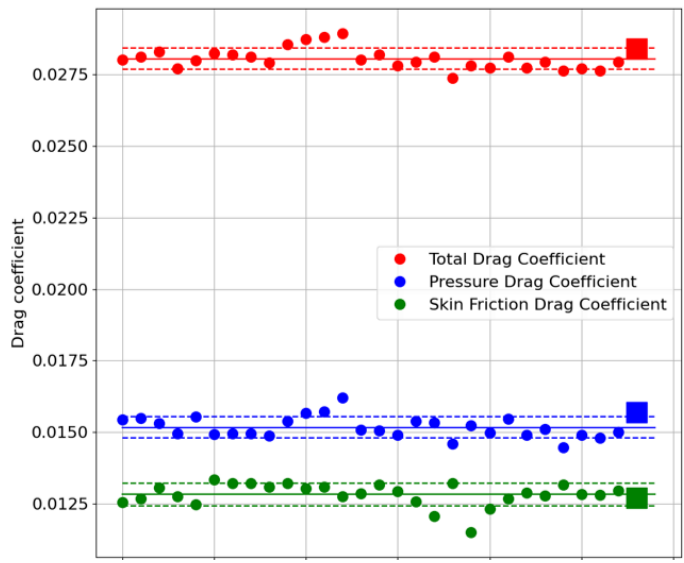


Fig. 5: Predicted total, pressure and skin friction drag coefficients. Results of other solvers from DPW6 are denoted by the smaller dots, while OpenFOAM results are represented by the larger squares on the right of the figure.

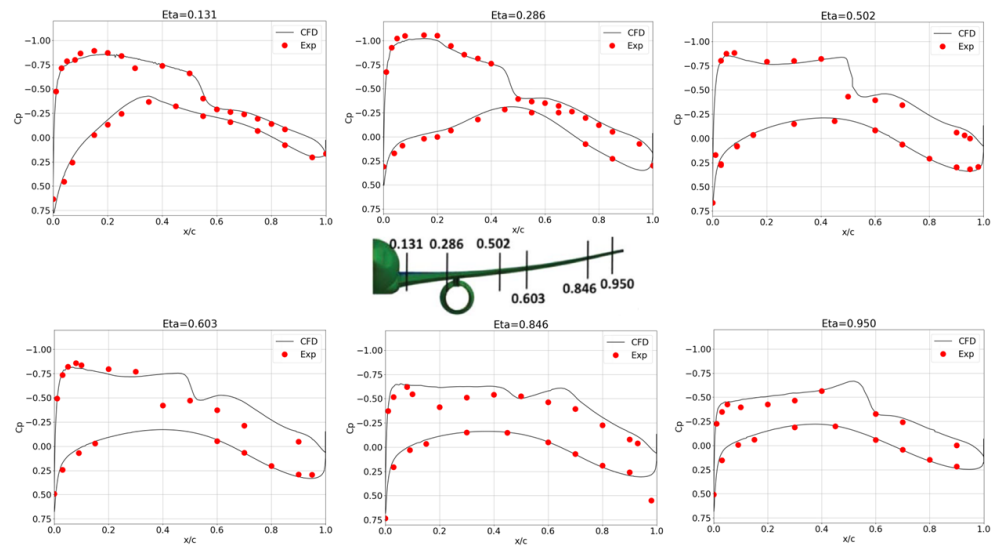


Fig. 6: Comparison of experimental and computational pressure coefficient at different wing spans for NASA CRM test case.

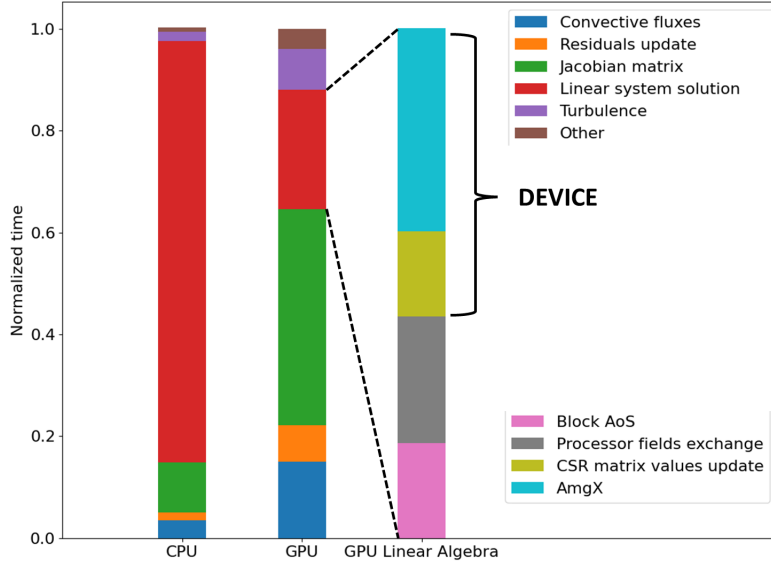


Fig. 7: Decomposition of CPU and GPU iterations for the NASA CRM test case. Times are normalized with respective total iteration times. Last bar chart represents decomposition of the linear algebra step on the GPU.

4.1.1 Performance assessment

Performance statistics are obtained as described in Sec. 3, and result from an average of measured computational times over 500 iterations after the solution was converged. Simulations statistics are shown in Table 2 in terms of total wall time and average on-chip memory usage per GPU. As already mentioned, linear algebra is typically one of the most cumbersome parts of the iteration in implicit solvers.

For the density-based solver, this is testified by the first bar in Fig. 7, showing the decomposition of a single iteration into its main computational kernels for the CPU version of the code. This figure reports the statistics obtained with the 260 million elements mesh simulation on 18 nodes (864 CPU cores + 72 GPUs) using GMRES with AMG preconditioner and DILU smoother as linear solver. We can see that almost 80% of the iteration is being spent solving the linear system. Although this is somewhat a pessimistic perspective for general calculations, due to the tight tolerance imposed on linear solver residuals (see Sec. 3), it can provide a good estimate for the initial phase of the simulation. Indeed, when the simulation is far from convergence and high Courant numbers are used (as typical of implicit solvers), the linear system becomes very stiff and a large number of iterations are needed, significantly impacting the total wall time. Instead, for the GPU-LA version, this is not the case. Indeed, linear system solution now makes for about 25% of the total iteration, while the most time consuming parts are related to the Jacobian matrix assembly and convective fluxes calculation. Please notice that for each bar, times are normalized with the corresponding total time relative to that bar. For the GPU-LA solution, linear algebra

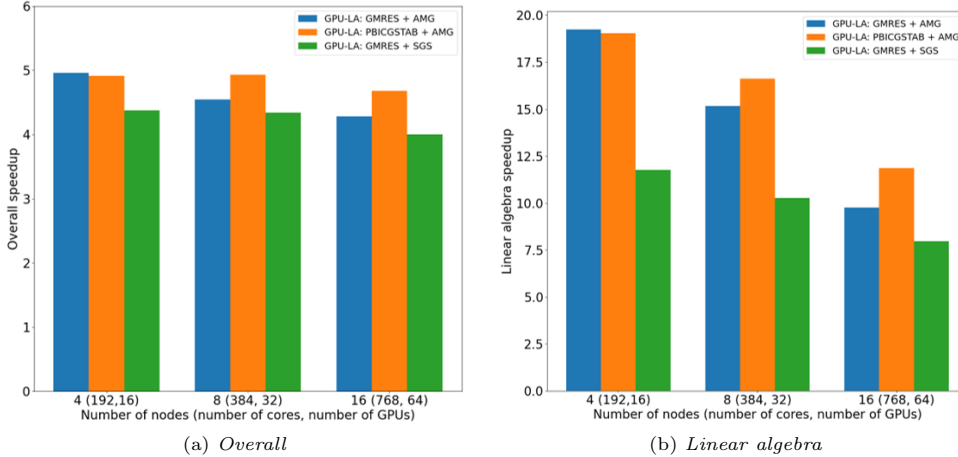


Fig. 8: Computational performance of GPU-LA in terms of speedup. Results are normalized with total iteration time (respectively, linear system solution time) for the CPU legacy case on the same number on nodes.

can be further decomposed in the preprocessing steps necessary to assemble and upload the matrix in the CSR format needed by AmgX and the actual iterative solution. The latter and the LDU to CSR conversion are performed on the device, while there is a significant overhead due to MPI ranks communication and matrix conversion into block AoS format. The figure clearly highlights a key point. First, future work should concentrate on other computational kernels, as further optimization of linear system solution would lead to a foreseeable performance improvement in the range of 10–15%. This would however require a much higher implementation effort, with the additional risk of penalizing platform portability and breaking compatibility with other software releases.

Fig. 8 shows the obtained speedup for the 45 million elements case and three different linear solvers, namely GMRES and PBiCGStab with AMG preconditioner, and GMRES with SGS preconditioner. The latter represents the configuration most similar to the one used in the CPU only version. Fig. 8a shows the overall speedup, while Fig. 8b represents the speedup obtained for linear algebra only, including the necessary preprocessing steps (red bar in Fig. 7). Results are presented for 4, 8 and 16 GPU nodes, and are normalized with total iteration time (respectively, linear system solution time) for the CPU legacy case on the same number on nodes. The overall simulation time is accelerated from 4 to 5 times, even as we approach the strong scalability limit on 16 nodes. In addition, as expected, the usage of multigrid preconditioner gives an edge compared to SGS, especially when the number of cells per GPU is higher. The obtained performance improvement makes the application of this method very appealing for coupled solvers.

Finally, Fig. 9 shows normalized iteration times on different numbers of nodes, where the dotted black line shows the ideal scalability trend. Reference is the total

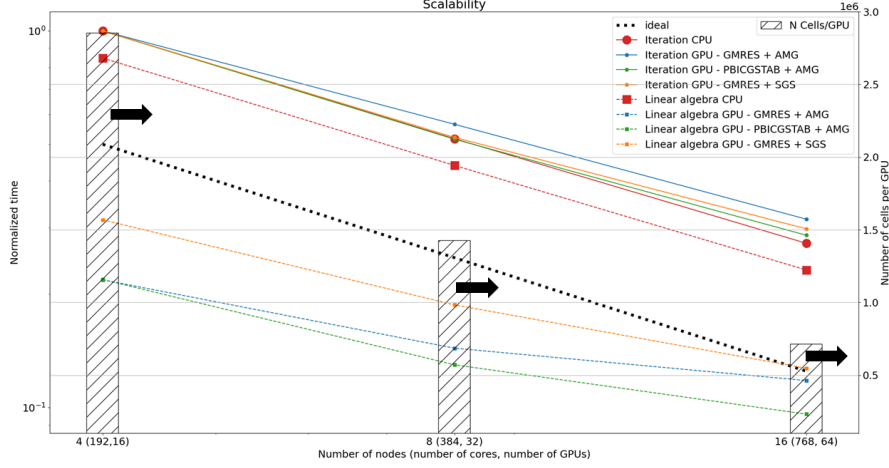


Fig. 9: Computational performance of GPU-LA in terms of scalability. Results are normalized with total iteration time for CPU legacy case on 4 nodes (192 cores).

iteration time for the 4 nodes CPU configuration. The bar charts represent the total number of cells per GPU. As can be seen, PBiCGStab has the best performance in terms of scalability among GPU solvers, showing a similar trend to the CPU solver, while for the four nodes case GMRES has a slight edge. Since the number of streaming multiprocessor in a single GPU is much higher than the number of CPU cores in a node, it is to be expected that GPU-LA reaches a strong scalability limit for a lower number of nodes than CPU only version. A number of cells around 1-5 million per GPU seems appropriate to exploit efficiently linear algebra acceleration.

Table 2 provides a quantitative overview of the computational performance of the density based solver. The wall time spent running 500 iterations is included for the CPU GMRES solver with LUSGS preconditioner, and for both the GMRES and PBiCGStab GPU solvers with AMG preconditioner. For the accelerated cases, the last column contains the maximum VRAM usage divided by the number of GPUs. These data can be employed to compare the ICSFoam performance with proprietary and open-source CFD software, demonstrating the general value of this research product. From an industrial perspective, the stability of the coupled formulation is extremely effective in relaxing the strict mesh requirements that come with standard OpenFOAM solvers. Furthermore, the GPU acceleration provides a performance boost that significantly lower the time-to-solution of applications typically encountered in the aerospace sector, such as the NASA CRM presented in this section. An interesting observation can be extrapolated from the maximum VRAM usage: the cases with 8 and 16 nodes are characterized by a low-to-medium GPU memory load, considering a 40 GB limit for NVIDIA A100 accelerators. Consequently, future studies might regard the investigation of different configurations to define the best compromise between hardware cost, computational performance and number of nodes.

Table 2: Computational times for NASA CRM simulations

Case	Solver	N GPUs	WT x 500 iter. [s]	Max VRAM / NGPUs [GB]
45 M - 4 nodes	CPU - GMRES + LUSGS	//	15996	//
	GPU - GMRES + AMG	16	3273	21.7
	GPU - PBiCGStab + AMG	16	3279	21.2
45 M - 8 nodes	CPU - GMRES + LUSGS	//	8268	//
	GPU - GMRES + AMG	32	1830	13.9
	GPU - PBiCGStab + AMG	32	1699	13.7
45 M - 16 nodes	CPU - GMRES + LUSGS	//	4330	//
	GPU - GMRES + AMG	64	1045	9.9
	GPU - PBiCGStab + AMG	64	964	9.7
260 M - 18 nodes	GPU - GMRES +AMG	72	7744	26.6

4.2 Test Case 2: incompressible DrivAer

The second test case presented involves the steady-state incompressible flow field around the notchback version of the DrivAer from the series of Automotive CFD Prediction Workshop [42]. The workshop focuses on a closed cooling configuration with static wheels and static floor. A comprehensive set of experimental data from the Pininfarina Wind Tunnel including aerodynamic forces and surface pressure measurements is available on the website. The high-Reynolds mesh generated by the workshop committee is used for the simulations. The domain is composed of a rectangular bounding box of extension $120\text{ m} \times 44\text{ m}$. The simulations are "free air" and do not include the wind tunnel geometry. The mesh, generated using ANSA BETA CAE, is composed of 128 million elements and has a $y^+ \approx 30$. A fixed velocity value of 38.89 m s^{-1} is imposed at the domain inlet, while a zero relative pressure is set at the outlet. Since the mesh was originally generated for scale-resolving DES simulations, no symmetry condition is imposed on the half plane and the full car span is modeled. On the upper and side domain surfaces, a slip condition is imposed. For RANS turbulence closure, the two-equations $k - \omega$ SST model [43] is used. Second order upwind schemes are used for convective fluxes.

Simulations were carried out with the coupled incompressible solver for 3000 iterations. Convergence was monitored by looking at integral aerodynamic coefficients and residuals. Due to massive flow separation in the car wake, a stationary solution could not be reached and flow statistics oscillates around a mean value. For this reason, comparison of velocity contours with experiments is performed using a velocity field averaged over the last 500 iterations.

In Fig. 10, the comparison of mean velocity contours on the side and in the main wake area is reported. A satisfactory agreement is found between CFD and experimental findings, including the side wake, wheels wake close to the ground, as well as the underbody wake in the rear part of the vehicle. The main features of the underbody flow are also correctly captures, as testified by Fig. 11. The extension of wheel wakes

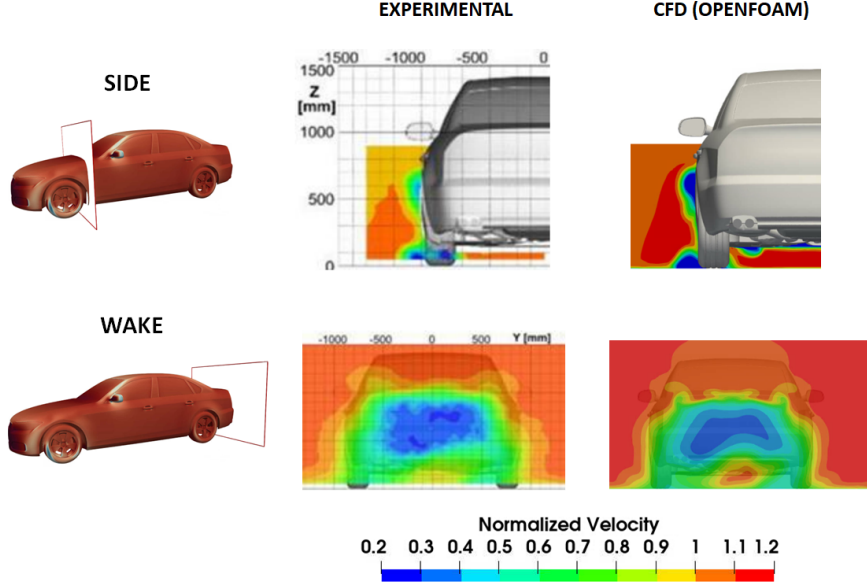


Fig. 10: Normalized velocity contours at different planes for the DrivAer test case. Experimental results from Hupertz *et al.*[44] are compared with OpenFOAM.

is comparable, although the front wheel wake is slightly deflected outboard. Experimental measurements from pressure probes on the symmetry plane are also available for the upperbody and the underbody of the vehicle. Probes locations are shown on the bottom of the plots in Fig. 12. As can be seen from the figure, there is a very good agreement with experimental values on both sides of the car, especially on the hood, where the flow is mostly attached to the wall. Pressure coefficient is slightly underpredicted on the roof, above the trunk and in the separation area in the underbody. Finally, in Fig. 13, drag, front and rear lift coefficients are compared with the ones obtained with commercial CFD solvers by other participants to the workshop. Standard deviation of values over last 500 iterations is also reported on the OpenFOAM bar. As can be noticed, there is a significant dispersion in the values obtained with CFD solvers. Drag values are within the 10% of experimental range, while a general disagreement between CFD lift coefficients and experimental data is obtained, especially for what concerns the front lift.

4.2.1 Performance assessment

This section includes a performance comparison between the coupled solver and the segregated pressure-based solver *simpleFoam* released with OpenFOAM vanilla. Simulations statistics are shown in Table 3 in terms of total wall time and average on-chip memory usage per GPU. Generally, the memory requirement is lower than the one of NASA CRM, due to the absence of the energy equation in the coupled system.

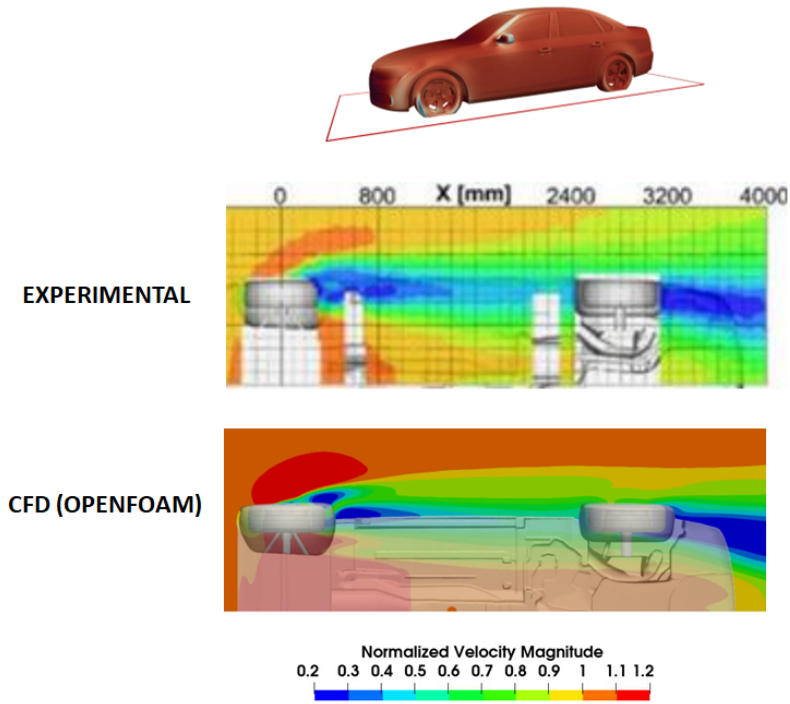


Fig. 11: Normalized velocity contours at different planes for the DrivAer test case. Experimental results from Hupertz *et al.*[44] are compared with OpenFOAM.

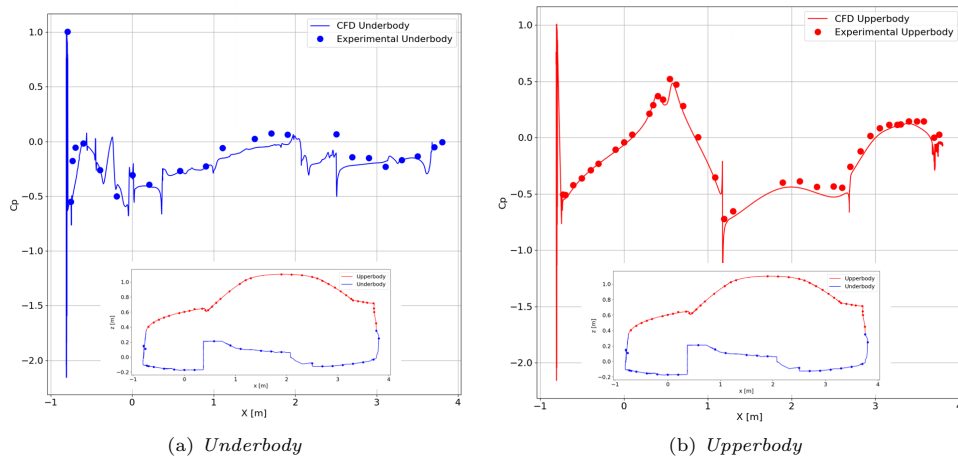


Fig. 12: Comparison of experimental and computational pressure coefficient on car symmetry plane at different probes location.

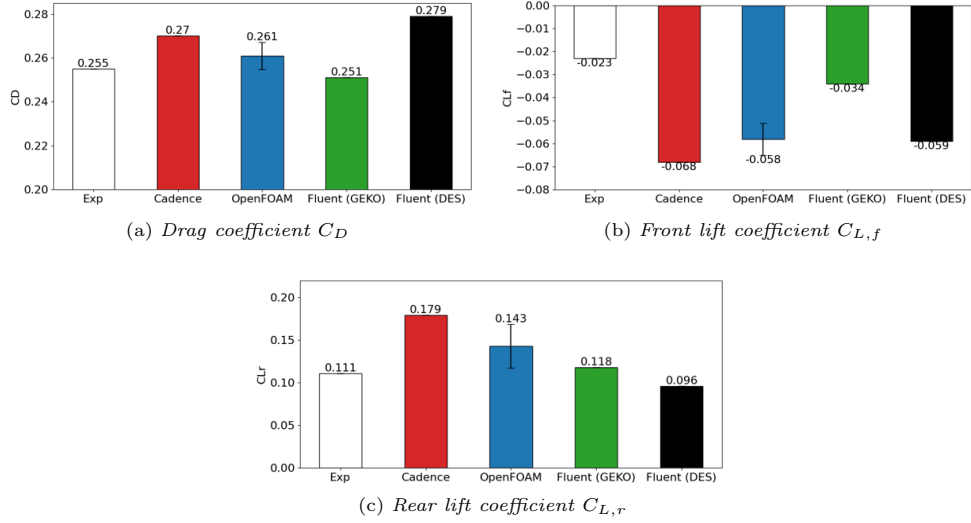


Fig. 13: Aerodynamic coefficients for the DrivAer case from 2nd Automotive CFD Workshop and OpenFOAM. Standard deviation of values over last 500 iterations is also reported on the OpenFOAM bar.

Table 3: Computational times for DrivAer simulations

Case	Solver	N GPUs	WT x 500 iter. [s]	Max VRAM / NGPUs [GB]
128 M - 8 nodes	CPU - Segregated	//	2389	//
	GPU - GMRES + AMG	32	2395	24.35
	GPU - PBiCGStab + AMG	32	2434	23.07
128 M - 16 nodes	CPU - Segregated	//	1378	//
	GPU - GMRES + AMG	64	1383	15.17
	GPU - PBiCGStab + AMG	64	1253	14.73

It must be remarked that convergence could not be obtained with *simpleFoam* due to stability issues, even employing first order schemes and very low relaxation factors. On the contrary, the coupled solver was characterized by a smooth convergence history, highlighting the strong benefits of a full pressure-velocity coupling. Therefore, to make comparisons, the simulation was run until convergence with the coupled solver and then for other 500 iterations with the SIMPLE approach to gather the statistics. For *simpleFoam*, the native Geometric Algebraic MultiGrid (GAMG) is used for the pressure equation, while PBiCGStab with DILU preconditioner is used for the momentum equation. Due to mesh non-orthogonality, the pressure correction equation is typically solved multiple times in the SIMPLE approach, so that explicit non orthogonal corrections can be included in the pressure-velocity coupling. In the present study, one

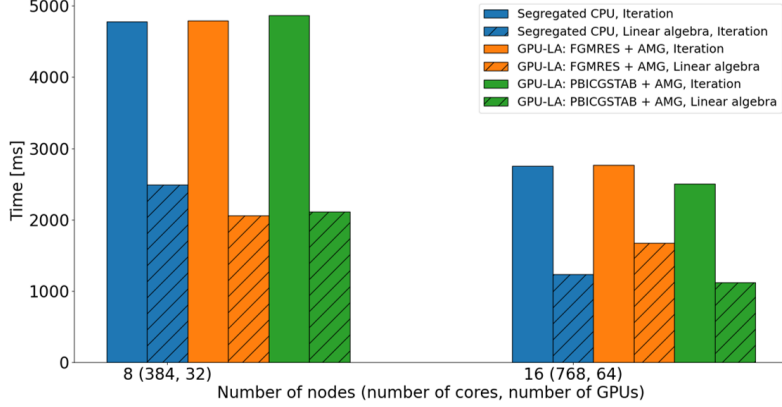


Fig. 14: Computational times for the Drivaer test case. Average times spent for the whole iteration as well as linear algebra only are shown for segregated CPU and GPU-LA configurations.

additional non-orthogonal correction was employed for the pressure equation. It is worthwhile to notice that segregated solvers usually present a significantly lower time per single iteration compared to the coupled approach. Fig. 14 shows that with GPU acceleration of linear algebra, the authors benefit from the stability of a fully implicit approach, still maintaining a time per iteration comparable, if not lower, to those of the segregated solver. As for the CRM simulation, the PBiCGStab solver shows better scalability compared to GMRES.

Fig. 15 illustrates the decomposition of the iteration for the two solvers into the main computational kernels. Times are again normalized with respect to the total iteration times. For *simpleFoam*, the iteration is simply composed of momentum predictor, pressure correction equation and turbulence solution. Pressure equation discretization and solution times in the first bar include also the non-orthogonal correction. For the coupled solver, about one third of the iteration is used to discretize and assemble the coupled matrix. The additional coupling terms need to be discretized as described in Sec. 2 and inserted in the matrix, leading to an overhead. This, however, is more than compensated by the faster linear algebra solution obtained through the offloading onto the device. With a two-equation turbulence model, the solution of k and ω represents approximately 25% of total iteration time.

Since convergence could not be obtained with the segregated solver, an additional test was performed to demonstrate the benefit of using a coupled solver with linear algebra offloading in terms of overall simulation performance. A coarser mesh of 22 million elements was generated using *snappyHexMesh*, the built-in OpenFOAM mesher. This tool is still far from being sustainable in industrial workflows, but allows to obtain a mesh with an improved quality according to OpenFOAM standards. Standard simulation settings were adopted, as previously described. Calculations were performed using a single GPU node, with 48 CPU cores and 4 GPUs (for coupled solver only). Fig. 16 shows the convergence of averaged aerodynamic coefficients versus total simulation times for the two solvers. A window average over 400 iterations was employed

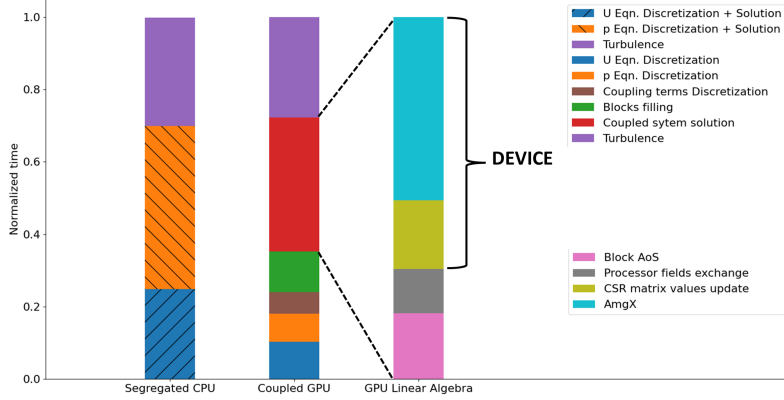


Fig. 15: Decomposition of CPU and GPU iterations for the DrivAer test case. Times are normalized with respective total iteration times. Last bar chart represents decomposition of the linear algebra step on the GPU.

in this case to assess the convergence of the solution. It can be seen that the coupled solver reaches a converged value of the average drag coefficient approximately three times faster than the segregated solver in terms of total wall time. Average lift coefficient also shows an improved convergence trend.

5 Conclusions

This paper has presented a workflow to extend a generic library for implicit coupled simulations through GPU acceleration of linear algebra. The OpenFOAM-based *ICSFoam* library for finite-volume discretization of coupled systems of PDEs, was coupled with NVIDIA AmgX through a modified version of the *amgx4Foam* library. This allowed to offload the most time consuming part of the iteration onto the accelerator while keeping the remaining part on the host, in a heterogeneous CPU/GPU architecture paradigm. We showed that significant performance speedups can be easily achieved. In particular, speedups of the order of $10 - 20x$ for the linear algebra only and $4 - 5x$ overall have been obtained. The offloading of sparse matrices for coupled linear systems gives in general better performance with respect to segregated solvers due to the more favourable arithmetic intensity of the block AoS structure, while retaining a low level of implementation effort. This fact, combined with the improved convergence and the inherent robustness and stability of coupled solvers, shows that this approach is suitable for industrial simulations of complex geometries. To prove this fact, we show the results for a compressible and incompressible test cases using pressure and density-based solvers, respectively.

Remarkably, this is the first implementation of GPU accelerated coupled implicit simulations in OpenFOAM, which is arguably the most widely employed open source CFD software in academic and industrial context. We highlighted that, with the current implementation, linear algebra of the coupled solver is not the most time-consuming part of the iteration anymore, weighting now for approximately $20 - 25\%$ of total wall

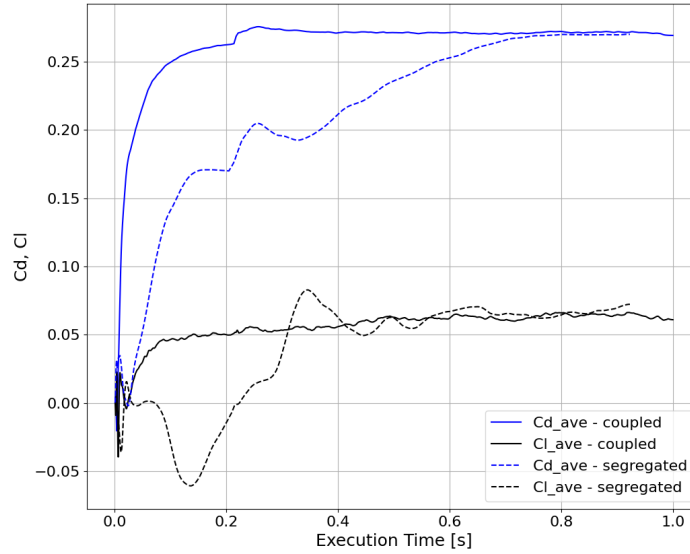


Fig. 16: Convergence of aerodynamic coefficients for the 22 M elements test. Coupled vs segregated solvers in terms of total simulation time.

time.

Therefore, future efforts to further accelerate the code need necessarily to focus on the offloading of the other computational kernels, such as discretization, fluxes calculation and turbulence equations. We also showed that, despite future generation GPU devices will feature more and more on-chip memory, VRAM can be still a critical issue for large-sized industrial problems. This can severely impact the minimum number of GPUs required for a single simulation, with consequent increase in the hardware cost. Optimization needs to be carried out to reduce the memory footprint of linear algebra algorithms.

Finally, we can expect even superior performances when CPU-GPU shared-memory architectures (e.g. NVIDIA Grace Hopper superchip) will be available, since memory copies between host and devices systems are no longer needed

Declarations

Conflict of interest

The authors declare no conflict of interest.

Availability of data and materials

The data presented in this study are available upon reasonable request from the corresponding author.

References

- [1] M.B. Rivers, A. Dittberner, Experimental investigations of the nasa common research model. *Journal of Aircraft* **51**(4), 1183–1193 (2014). <https://doi.org/10.2514/1.C032626>
- [2] D. Wood, M.A. Passmore, A.K. Perry, Experimental Data for the Validation of Numerical Methods - SAE Reference Notchback Model. *SAE International Journal of Passenger Cars - Mechanical Systems* **7**(1), 145–154 (2014). <https://doi.org/https://doi.org/10.4271/2014-01-0590>
- [3] J.M. Cebri'n, G.D. Guerrero, J.M. García, in *2012 IEEE 26th International Parallel and Distributed Processing Symposium Workshops & PhD Forum* (2012), pp. 1014–1022. <https://doi.org/10.1109/IPDPSW.2012.124>
- [4] D. Price, M. Clark, e.a. Barsdell, B.R., Optimizing performance-per-watt on GPUs in high performance computing. *Comput Sci Res* **31**, 185–193 (2016). <https://doi.org/https://doi.org/10.1007/s00450-015-0300-5>
- [5] A. Krzywaniak, P. Czarnul, J. Proficz, Dynamic gpu power capping with online performance tracing for energy efficient gpu computing using depo tool. *Future Generation Computer Systems* **145**, 396–414 (2023). <https://doi.org/https://doi.org/10.1016/j.future.2023.03.041>
- [6] Ansys. Fluent Fluid Simulation Software (2023). <https://www.ansys.com/products/fluids/ansys-fluent> [Accessed: Dec 2023]
- [7] SIEMENS. Simcenter STAR-CCM+ CFD software (2023). <https://plm.sw.siemens.com/en-US/simcenter/fluids-thermal-simulation/star-ccm/> [Accessed: Dec 2023]
- [8] M. Naumov, M. Arsaev, P. Castonguay, J. Cohen, J. Demouth, J. Eaton, S. Layton, N. Markovskiy, I. Regul, N. Sakharnykh, V. Sellappan, R. Strzodka, Amgx: A library for gpu accelerated algebraic multigrid and preconditioned iterative methods. *SIAM Journal on Scientific Computing* **37**(5), S602–S626 (2015). <https://doi.org/10.1137/140980260>
- [9] F. Piscaglia, F. Ghioldi, GPU Acceleration of CFD Simulations in OpenFOAM. *Aerospace* **10**(9) (2023). <https://doi.org/10.3390/aerospace10090792>
- [10] J. Williams, C. Sarofeen, H. Shan, M. Conley, An accelerated iterative linear solver with gpus for cfd calculations of unstructured grids. *Procedia Computer*

- Science **80**, 1291–1300 (2016). <https://doi.org/https://doi.org/10.1016/j.procs.2016.05.504>. International Conference on Computational Science 2016, ICCS 2016, 6-8 June 2016, San Diego, California, USA
- [11] X. Zhang, X. Guo, Y. Weng, X. Zhang, Y. Lu, Z. Zhao, Hybrid mpi and cuda paralleled finite volume unstructured cfd simulations on a multi-gpu system. *Future Generation Computer Systems* **139**, 1–16 (2023). <https://doi.org/https://doi.org/10.1016/j.future.2022.09.005>
- [12] S. Jaiswal, R. Reddy, R. Banerjee, S. Sato, D. Komagata, M. Ando, J. Okada, in *2016 IEEE 23rd International Conference on High Performance Computing Workshops (HiPCW)* (2016), pp. 81–89. <https://doi.org/10.1109/HiPCW.2016.020>
- [13] J.H. Ferziger, M. Perić, R.L. Street, *Computational Methods for Fluid Dynamics*, 4th edn. (Springer, 2020)
- [14] M.B. L. Mangani, M. Darwish, Development of a novel fully coupled solver in openfoam: Steady-state incompressible turbulent flows. *Numerical Heat Transfer, Part B: Fundamentals* **66**(1), 1–20 (2014). <https://doi.org/10.1080/10407790.2014.894448>
- [15] M.D. L. Mangani, F. Moukalled, An openfoam pressure-based coupled cfd solver for turbulent and compressible flows in turbomachinery applications. *Numerical Heat Transfer, Part B: Fundamentals* **69**(5), 413–431 (2016). <https://doi.org/10.1080/10407790.2015.1125212>
- [16] M. Darwish, L. Mangani, F. Moukalled, Implicit boundary conditions for coupled solvers. *Computers & Fluids* **168**, 54–66 (2018)
- [17] "<https://www.nvidia.com/it-it/data-center/h100>". NVIDIA GPU H100 Tensor Core
- [18] H.G. Weller, G. Tabor, H. Jasak, C. Fureby, A tensorial approach to computational continuum mechanics using object-oriented techniques. *Computers in Physics* **12**(6), 620–631 (1998)
- [19] "<https://www.esi-group.com/customer-successes/audi-maximizes...>". Audi Maximizes the Driving Range and Acoustic Quality of the New e-tron Using ESI Virtual Prototyping Solutions
- [20] S. Oliani, N. Casari, M. Carnevale, Icsfoam: An openfoam library for implicit coupled simulations of high-speed flows. *Computer Physics Communications* **286**, 108673 (2023). <https://doi.org/10.1016/j.cpc.2023.108673>
- [21] T. Uroić, H. Jasak, Parallelisation of selective algebraic multigrid for block–pressure–velocity system in openfoam. *Computer Physics Communications*

- 258**, 107529 (2021). <https://doi.org/https://doi.org/10.1016/j.cpc.2020.107529>
- [22] M. Darwish, I. Sraj, F. Moukalled, A coupled finite volume solver for the solution of incompressible flows on unstructured grids. *Journal of Computational Physics* **228**(1), 180–201 (2009). <https://doi.org/https://doi.org/10.1016/j.jcp.2008.08.027>
- [23] ESI OpenCFD OpenFOAM. <http://www.openfoam.com/>
- [24] The OpenFOAM Foundation. <http://www.openfoam.org/dev.php>
- [25] F. Ghioldi, F. Piscaglia, Acceleration of supersonic/hypersonic reactive CFD simulations via heterogeneous CPU-GPU supercomputing. *Computers & Fluids* **266**, 106041 (2023). <https://doi.org/https://doi.org/10.1016/j.compfluid.2023.106041>
- [26] J. Heyns, O. Oxtoby, Modelling high-speed viscous flow in openfoam®. 9th South African Conference on Computational and Applied Mechanics, SACAM 2014 (2014)
- [27] S. Oliani, N. Casari, M. Carnevale, A new framework for the harmonic balance method in openfoam. *Machines* **10**(4) (2022)
- [28] E. Fadiga, F. Rondina, S. Oliani, T. Benacchio, D. Malacrida, L. Capone, (2023). <https://doi.org/10.23967/c.coupled.2023.018>
- [29] Y. Saad, M.H. Schultz, Gmres: a generalized minimal residual algorithm for solving nonsymmetric linear systems. *Siam Journal on Scientific and Statistical Computing* **7**, 856–869 (1986)
- [30] A. Jameson, W. Schmidt, E. Turkel, Solutions of the euler equations by finite volume methods using runge-kutta time-stepping schemes. *AIAA paper* **1259** (1981)
- [31] H. Luo, J.D. Baum, R. Löhner, A fast, matrix-free implicit method for compressible flows on unstructured grids. *Journal of Computational Physics* **146**(2), 664–690 (1998)
- [32] J. Blazek, *Computational Fluid Dynamics: Principles and Applications*, 3rd edn. (Butterworth-Heinemann, 2015)
- [33] S. Patankar, *Numerical Heat Transfer and Fluid Flow*, 1st edn. (Taylor and Francis Group, 1980)
- [34] R. Issa, Solution of the implicitly discretised fluid flow equations by operator-splitting. *Journal of Computational Physics* **62**(1), 40–65 (1986)
- [35] C.M. Rhie, W.L. Chow, Numerical study of the turbulent flow past an airfoil with trailing edge separation. *AIAA Journal* **21**(11), 1525–1532 (1983). <https://doi.org/10.2514/6.1983-1152>

[//doi.org/10.2514/3.8284](https://doi.org/10.2514/3.8284)

- [36] M. Martineau, S. Posey, F. Spiga, in *8th OpenFOAM Conference* (2020)
- [37] "<https://www.leonardo.com/en/innovation-technology/davinci-1>". Supercomputer davinci-1
- [38] J. Vassberg, M. Dehaan, M. Rivers, R. Wahls, in *26th AIAA Applied Aerodynamics Conference* (2008). <https://doi.org/10.2514/6.2008-6919>
- [39] E.N. Tinoco, O.P. Brodersen, S. Keye, K.R. Laffin, E. Feltrop, J.C. Vassberg, M. Mani, B. Rider, R.A. Wahls, J.H. Morrison, D. Hue, C.J. Roy, D.J. Mavriplis, M. Murayama, Summary data from the sixth aiaa cfd drag prediction workshop: Crm cases. *Journal of Aircraft* **55**(4), 1352–1379 (2018). <https://doi.org/10.2514/1.C034409>
- [40] "<https://aiaa-dpw.larc.nasa.gov/Workshop6/workshop6.html>". 6th AIAA CFD Drag Prediction Workshop
- [41] P. Spalart, S. Allmaras, *A one-equation turbulence model for aerodynamic flows* (1992). <https://doi.org/10.2514/6.1992-439>
- [42] <https://autocfd.eng.ox.ac.uk/>. Automotive CFD Prediction Workshop
- [43] F.R. Menter, M. Kuntz, R. Langtry, Ten years of industrial experience with the sst turbulence model. *Turbulence, heat and mass transfer* **4**(1), 625–632 (2003)
- [44] B. Hupertz, K. Chalupa, L. Krueger, K. Howard, H.D. Glueck, N. Lewington, J.H. Chang, Y.s. Shin, (2021). <https://doi.org/10.4271/2021-01-0958>